REVIEW

Cavity-Enhanced Excitation of Molecules with Continuous-wave Lasers†

Cun-Feng Cheng[a*], Shui-Ming Hu[b*]

a. Hefei National Research Center for Physical Sciences at the Microscale, University of Science and Technology of China, Hefei 230026, China
b. State Key Laboratory of Chemical Reaction Dynamics, University of Science and Technology of China, Hefei 230026, China

(Dated: Received on November 20, 2025; Accepted on January 12, 2026)

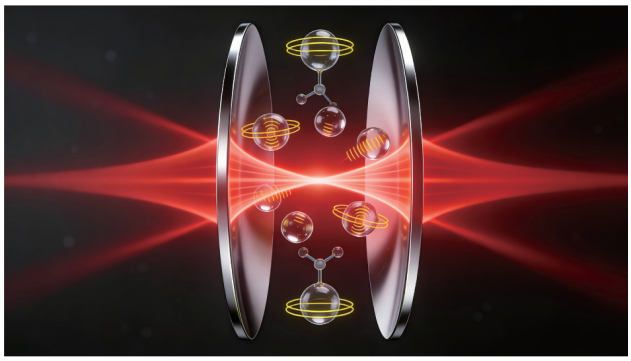

The precise excitation of molecular vibrational states is critical for advancing chemical dynamics, precision spectroscopy, and trace gas sensing. This objective, however, is often hindered by the weak oscillator strengths of ro-vibrational transitions, which render conventional continuous-wave (cw) lasers ineffective due to their limited power. This fundamental challenge is overcome by cavity-enhanced excitation (CEE), a technique that locks a cw laser to a high-finesse optical cavity. This configuration amplifies the intra-cavity light intensity by several orders of magnitude while preserving a narrow spectral linewidth. The resulting synergy enables highly efficient, state-selective population transfer and high-resolution spectroscopy previously considered impractical. This review elucidates the core technique of laser-cavity locking and highlights its applications, notably in the quantitative detection of trace isotopes and the investigation of highly excited vibrational states with kilohertz-level accuracy.

Key words: Cavity-enhanced excitation, Rovibrational spectroscopy, Laser spectroscopy, Two-photon spectroscopy

I. INTRODUCTION

The interaction between light and molecules serves as the cornerstone for manipulating and probing quantum states in molecular systems. When resonant with molecular transitions, light can efficiently promote molecules to excited states, enabling not only spectroscopic characterization but also controlled state preparation and dynamical studies [1]. This excitation process forms the basis for exploring energy transfer pathways, reaction dynamics [2, 3], and quantum state manipulation across chemical physics [3, 4]. The choice of excitation source presents a fundamental trade-off in molecular studies. Pulsed lasers with high peak powers can achieve substantial excitation but suffer from broad spectral linewidths that preclude precise quantum state selection [2, 5, 6]. Conversely, single-frequency continuous-wave (cw) lasers offer the spectral purity necessary for state-selective excitation [7], yet their typical milliwatt-level powers are usually insufficient for efficient population transfer in single-pass configurations. This limitation becomes particularly severe for weak transitions to highly excited states or in dilute molecular samples.

Cavity-enhanced excitation (CEE) techniques overcome this limitation by dramatically extending the ef-

† Part of Special Issue dedicated to Professor Qing-Shi Zhu on the occasion of his 80th birthday.

* Authors to whom correspondence should be addressed.
E-mail: cfcheng@ustc.edu.cn, smhu@ustc.edu.cn

 © 2026 Chinese Physical Society

fective interaction path between light and molecules [8]. In a high-finesse optical cavity formed by ultra-reflective mirrors, cw laser light undergoes thousands to millions of round trips, leading to an intensity buildup of several orders of magnitude while retaining the narrow spectral linewidth essential for quantum-state resolution [9]. This effective power enhancement elevates milliwatt-level cw lasers into versatile tools for high-resolution molecular studies, enabling a range of advanced applications including double-resonance spectroscopy with kilohertz accuracy [10], state-selective population transfer [11], state-resolved reaction dynamics [12–14], and coherent manipulation of molecular quantum states [6, 15].

By transforming conventional cw lasers into efficient sources for quantum-state-resolved studies, CEE methods have established a critical experimental platform that bridges high-resolution spectroscopy and chemical dynamics. This review systematically examines their fundamental principles, experimental implementations, and transformative impact in modern molecular science. The review is organized as follows: Section II introduces the fundamental technique of coupling a cw laser into a resonant optical cavity. Section III presents representative applications of CEE in two-level systems, including saturation spectroscopy and population transfer in molecular beams. Section IV explores advanced implementations of CEE in three-level systems, and the final section offers perspectives on future developments.

II. LIGHT IN A HIGH-FINESSE CAVITY

For a resonant cavity composed of two identical high-reflectivity (HR) mirrors, the reflectivity of the mirror and the cavity finesse $\mathcal{F}$ are:

$$\begin{aligned} r &= 1 - t - \ell, \\ \mathcal{F} &= \frac{\pi}{t + \ell + \alpha L}, \end{aligned} \tag{1}$$

where t and ℓ are the transmittance and loss of a single HR mirror, α is the sample absorption coefficient, and L is the cavity length. The laser power injected to the cavity (P_{in}), circulating power inside the cavity (P_{c}), and transmitted power from the cavity (P_{t}) fulfill the equations [8, 16]:

$$\begin{aligned} \frac{P_{\mathrm{t}}}{P_{\mathrm{c}}} &= t, \\ \frac{P_{\mathrm{t}}}{P_{\mathrm{in}}} &= \frac{t^2}{(t + \ell + \alpha L)^2} = T, \end{aligned} \tag{2}$$

where T is the transmittance of the cavity. Note that the reflectivity of the HR mirror can be determined experimentally by measuring the ring-down time [17, 18] of the empty cavity ($\alpha = 0$):

$$c\tau_0 = \frac{L}{\ln(1/r)} \approx \frac{L}{1 - r}. \tag{3}$$

Therefore, the mirror loss (ℓ) can also be determined experimentally by measuring the transmittance of the empty cavity using Eqs. (2) and (3). Note that this measurement requires the laser to be locked to a cavity resonance.

Nowadays, high-reflectivity mirrors with $r > 0.9999$ are commercially available across the infrared to visible spectrum, with developments extending into the mid-infrared and ultraviolet. Such mirrors enable cavity ring-down times of several hundred microseconds, corresponding to tens of thousands of round trips within the resonator. This extensive multipass effect yields two major advantages: (i) an enhancement of the effective interaction path length by over four orders of magnitude, and (ii) a buildup of intra-cavity laser power by several thousandfold, provided that low mirror loss is maintained.

However, coupling a cw laser into a high-finesse resonant cavity is challenging. For example, in a 100-cm-long cavity with a finesse of 30,000, the width of a longitudinal mode is only about 5 kHz — significantly narrower than the typical linewidths of most free-running commercial diode lasers, which usually range from tens of kilohertz to a few megahertz. To match the cavity mode to the laser frequency, Romanini *et al.* [19] introduced a "dither-mirror" technique by scanning the cavity length, which later became widely adopted in cw-CRDS systems across many research groups [20–25]. Another approach, referred to here as the "dither-laser" method, involves rapidly dithering the laser frequency while keeping the cavity length fixed [26–28]. Both of these techniques force the laser to periodically resonate with the optical cavity by quickly modulating either the cavity length or the laser frequency. Although relatively simple to implement, they suffer from low efficiency. Because the laser frequency or cavity length is continuously scanned, the duration over which resonance is maintained is limited. As a result, the resonance condition can be lost before sufficient laser power builds up inside the cavity, leading to low and unstable transmitted light amplitudes. A solution to this problem is to ac-

DOI: 10.1063/1674-0068/cjcp2511176 © 2026 Chinese Physical Society

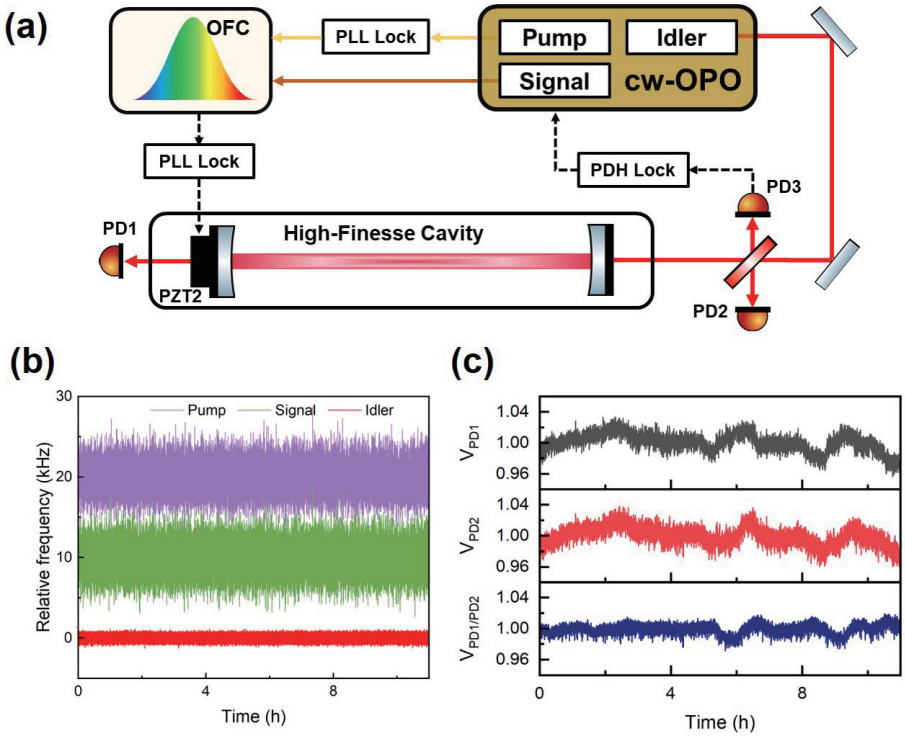

FIG. 1 (a) Schematic diagram of an example of mid-infrared laser locking to a high-finesse cavity. PLL: phase lock loop; PD: photo diode; OFC: optical frequency comb; OPO: optical parametric oscillator; PDH: Pound–Drever–Hall. (b) The frequency stability of the lasers after the frequency locking. The pump, signal and idler denote the pump, signal, and idler lights of the OPO, respectively. To display it more clearly, we shifted the frequency of the signal and pump lights by 10 kHz and 20 kHz, respectively. (c) The power stability of the lasers after the frequency locking. The signal monitored by PD1 and PD2 are normalized, and their division is shown in the lower panel.

tively lock the probe laser to the optical cavity to maintain resonance. When the locking servo is engaged, the cavity transmittance rapidly reaches a steady state, as described by Eq.(2). Typically, a fast servo loop with a bandwidth greater than 100 kHz is used to lock the laser frequency to the cavity via the Pound–Drever–Hall (PDH) technique [29]. If necessary, a slower servo can also be applied to stabilize the cavity length. In this configuration, both the cavity modes and the laser frequency remain stabilized, allowing the circulating laser power inside the cavity to be maintained at a high level.

Thanks to advances in laser locking technology, it has become increasingly straightforward to lock lasers to high-finesse optical cavities. FIG. 1(a) illustrates the frequency stabilization of a mid-infrared (MIR) laser source to a high-finesse optical cavity. The MIR radiation, generated by a continuous-wave optical parametric oscillator (cw-OPO) configured as in previous studies [30–32], delivered several hundred milliwatts across the 2.6−4.5 μm range. This output was coupled into a 75-cm-long high-finesse cavity formed by two high-reflectivity mirrors ($R \approx 99.967\%$) with 1-m radii of curvature, producing a Gaussian beam waist of 0.7 mm at the focus. Frequency stabilization was implemented via the PDH technique. The resulting error signal was fed back to the frequency of the OPO's near-infrared signal output, maintaining resonance between the MIR radiation and a longitudinal cavity mode. The cavity was housed in a vacuum chamber with active temperature stabilization to minimize frequency drift. Under locked conditions, the system exhibited a ring-down time of 7.7 μs and a transmittance of 1.1%, corresponding to an intra-cavity power enhancement factor of approximately 330 relative to the incident power.

The mid-infrared frequency was derived as the difference between the pump and signal frequencies, both of which were referenced to an optical frequency comb (OFC) disciplined by an active hydrogen maser with a fractional accuracy of 1.2×10^{-13}. The pump laser was first phase-locked to the OFC via a beat-lock servo. The frequency offsets of the pump and signal lasers from their respective comb lines, denoted Δf_{p} and Δf_{s}, were recorded, and their difference $(\Delta f_{\mathrm{p}} - \Delta f_{\mathrm{s}})$ served as the input to a phase-locked loop (PLL). The PLL generated a feedback signal applied to a piezoelectric actuator on one cavity mirror to stabilize the cavity length [33].

DOI: 10.1063/1674-0068/cjcp2511176 © 2026 Chinese Physical Society

A microwave function generator supplied the PLL reference, enabling precise control and determination of both the cavity length and the absolute MIR frequency.

Following frequency lock acquisition, laser stability was evaluated by recording the beat note between the laser and the OFC, as shown in FIG. 1(b). For clarity, the signal and pump frequencies were shifted by 10 kHz and 20 kHz, respectively. Within the OPO, the signal beam inherits the frequency stability of the pump laser, while the idler (MIR) exhibits superior stability due to common-mode noise suppression inherent in the difference-frequency generation process. Power stability was monitored using photodetectors PD1 and PD2, placed before and after the cavity, respectively, as plotted in FIG. 1(c). The transmitted power (PD1) closely tracked the input power (PD2), indicating that after frequency locking, power fluctuations predominantly originated from the laser source rather than from cavity misalignment or length variations.

III. CEE IN A TWO-LEVEL SYSTEM

A. Saturation spectroscopy

Saturation spectroscopy, by measuring the Lamb dips, stands as the most widely employed technique for overcoming the Doppler limit and determining precise spectral line positions. However, its application to molecular ro-vibrational transitions faces a fundamental challenge: these transitions typically exhibit weak oscillator strengths, requiring saturation intensities that often exceed the power capabilities of conventional tunable lasers. The integration of high-finesse optical cavities effectively addresses this limitation. In cavity-enhanced spectroscopy, such cavities serve a dual purpose: they not only dramatically improve detection sensitivity through multipass absorption but also generate substantial intra-cavity power buildup. This power enhancement creates the strong electromagnetic fields necessary to saturate weak molecular transitions, thereby enabling sub-Doppler resolution in systems where traditional saturation spectroscopy would be impractical.

When the laser is coupled into the cavity, the gas interacts with intra-cavity radiation in a TEM_{00} mode with intensity I and power $P = \dfrac{\pi w^2}{2} I$, where w is the beam waist along the transverse direction. The saturation intensity of an infrared transition can be calculated as [34]:

$$I_s = \frac{hc}{3}\frac{k^3}{A}(\Gamma + \gamma p)^2, \tag{4}$$

where h is the Planck constant, c is the speed of light, k is the wave vector of the transition, A is the Einstein A-coefficient of the transition, and $\Gamma + \gamma p$ is the homogeneous broadened width (FWHM) of the absorption line with the collision-induced broadening coefficient γ and sample pressure p. The saturation parameter is defined as $s = I/I_s$.

We neglect the spatial modulation effects of the standing-wave field inside the optical cavity and assume a spatially averaged saturation profile for molecules interacting with the light field. Under homogeneous broadening induced by the laser field, the absorption coefficient is modified as:

$$\alpha = \frac{\alpha_0}{\sqrt{1+s}}, \tag{5}$$

where α_0 denotes the non-saturated absorption coefficient. To account for saturation effects in cavity-enhanced measurements, the saturated-absorption cavity ring-down (SCAR) technique was developed, which extracts the intrinsic absorption signal by correcting for saturation-induced distortion, thereby improving the sensitivity of cavity ring-down spectroscopy [34].

The depth of the resulting Lamb dip depends on both the non-saturated absorption coefficient and the saturation parameter, as given by [8]:

$$\mathcal{D} = \alpha_0 \left(\frac{1}{\sqrt{1+s}} - \frac{1}{\sqrt{1+2s}} \right). \tag{6}$$

Since the saturation parameter s varies with sample pressure for a given molecular transition, Eq.(6) allows the Lamb-dip depth to be calculated across different pressure conditions.

Cavity-enhanced saturated absorption spectroscopy has enabled precise measurements of weak molecular ro-vibrational transitions [16, 33–36]. Representative spectra in FIG. 2 display Lamb dips of the R(10) line in the (3-0) band of CO measured at various pressures [33]. The dip depth reaches its maximum at 0.5 Pa and subsequently decreases with increasing pressure. The observed linewidth is primarily composed of a transit-time broadening contribution of approximately 130 kHz, combined with additional collision-induced broadening components. It is worth noting that the collision-in-

DOI: 10.1063/1674-0068/cjcp2511176 © 2026 Chinese Physical Society

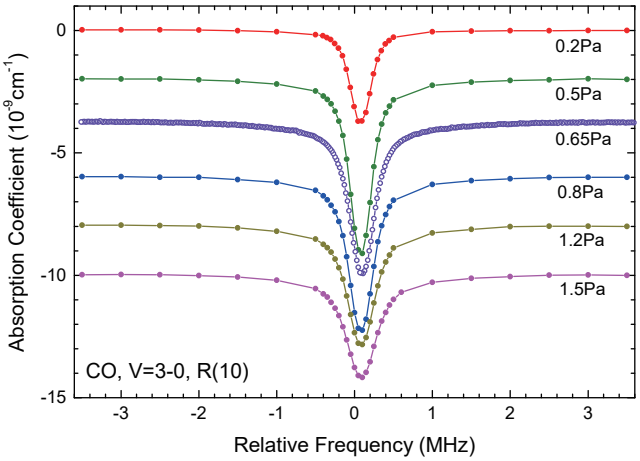

FIG. 2 Cavity ring-down saturation spectra of the R(10) line in the (3-0) band of $^{12}C^{16}O$ recorded under different sample pressures. Spectra were vertically shifted for better illustration. Reproduced with permission from Ref.[33]. Copyright 2017 AIP Publishing.

duced broadening of the Lamb dips was found [37, 38] to be much larger than that observed in Doppler-broadened spectra. Such broadening would considerably affect the saturation intensity and consequently change the Lamb-dip depth according to Eq.(6).

Among different molecular systems, hydrogen deuteride (HD) stands out as an ideal candidate for fundamental studies. Saturation absorption spectroscopy, as a high-resolution technique, has played a significant role in revealing the unusual lineshapes of HD. This is of particular importance because HD molecular transitions are crucial for precise molecular measurements and tests of fundamental physics. As a simple few-body system, its properties can be precisely calculated using quantum electrodynamics with fundamental constants. Unlike homonuclear H_2 and D_2, HD exhibits relatively strong dipole transitions in the near-infrared region. The Hefei group pioneered cavity ring-down Lamb-dip spectroscopy of HD, achieving approximately 200 W of intra-cavity power from a 10 mW diode laser input through a high-finesse cavity ($F \approx 1.2 \times 10^5$). For the R(1) line in the $V = 2 \leftarrow 0$ band, this configuration produced a saturation parameter of 0.001 and revealed a Lamb dip with a depth of 5×10^{-12} cm^{-1} and a width of 0.9 MHz, enabling determination of the line center with uncertainty below 0.1 MHz [39], representing one of the weakest molecular transitions measured via saturated absorption spectroscopy at that time. Independent investigation by the Amsterdam group using noise-immune cavity-enhanced optical heterodyne molecular spectroscopy (NICE-OHMS) yielded a line center frequency differing by 0.9 MHz from the Hefei result [40, 41]. Both groups observed asymmetric line shapes in HD spectra [42, 43], though they proposed different interpretations. The Hefei group attributed the asymmetry to Fano-like resonances arising from coupling between far-detuned electronic transitions and the standing-wave field [44], while the Amsterdam group emphasized the role of intermolecular interactions and hyperfine structure. This has led the latter group to focus on isotopologues with simpler hyperfine patterns [45] and quadrupole transitions [46]. Resolving these spectral discrepancies remains crucial for advancing precision measurements in molecular hydrogen systems as experimental capabilities continue to improve [47].

B. CEE in a molecular beam

Efficient state-selective excitation of molecules in a supersonic molecular beam is essential for state-to-state reaction dynamics researches and the elucidation of complex reaction mechanisms [48–53]. In particular, the excitation of molecules to higher ro-vibrational states stands at the forefront of current research, providing insight into unique reaction dynamics not observable at lower energy levels [54–56]. The cavity enhancement technique enables effective excitation and preparation of molecules in specific vibrationally excited states by significantly increasing population transfer under strong infrared laser irradiation, an essential capability for studies in chemical kinetics and reaction dynamics involving vibrationally excited species. In a non-adiabatic interaction scheme between molecules and infrared light, the excited-state population fraction in a two-level system can be described as:

$$\frac{n^*}{n_0} = \frac{s}{2(1+s)} \tag{7}$$

where n^* and n_0 denote the number of molecules in the excited state and the total number of molecules, respectively. A major challenge in achieving high population transfer efficiency lies in the high saturation intensity typically required for overtone transitions. For instance, the $(v = 3, j = 2) \leftarrow (v = 0, j = 1)$ transition in CO has a saturation intensity of 74 kW/cm^2, making direct infrared excitation into high vibrational states particularly difficult.

Nanosecond pulsed lasers with peak intensities exceeding 100 kW/cm^2 have been employed to drive infrared transitions, enabling vibrational excitation of CO

DOI: 10.1063/1674-0068/cjcp2511176 © 2026 Chinese Physical Society

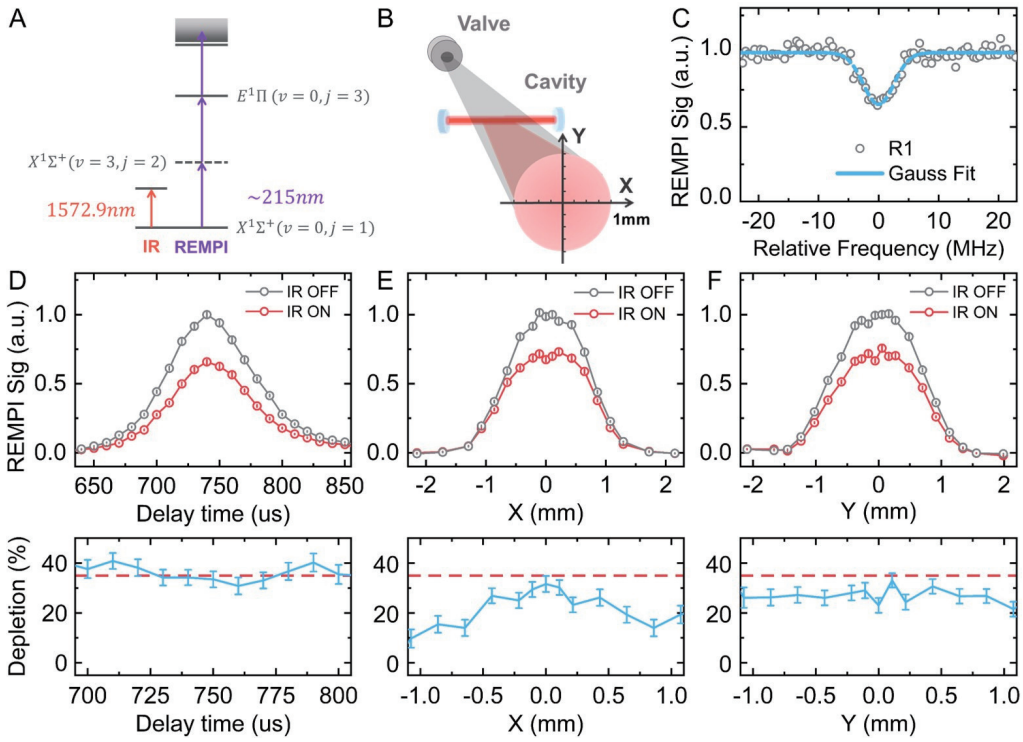

FIG. 3 (A) Energy levels of CO and the depletion scheme of the experiment. (B) The schematic drawing of the geometrical relation of the excitation laser and the transverse number density distribution of molecules in the vibrationally excited (red shadow) states. (C) The REMPI depletion spectrum obtained by scanning the IR laser frequency. (D) Upper panel: the TOF signal of the molecular beam with the IR ON (red) and OFF (black). Note that the *X*-axis of the graph is expressed with the speed of the molecular beam multiplied by the delay time. (E) Upper panel: the REMPI signal when scanning the position of the REMPI laser beam along the *X*-axis with the IR ON (red) and OFF (black). (F) Upper panel: the REMPI signal when scanning the position of the REMPI laser beam along the *Y*-axis with the IR ON (red) and OFF (black). Data in (D), (E), and (F) were measured with the IR frequency locked on-resonance with the $(v=3, j=2) \leftarrow (v=0, j=1)$ transition, and the lower panels show the corresponding depletion signal. The red dashed lines in (D), (E), and (F) indicate the population transfer efficiency of 35%, corresponding to the on-resonance population transfer efficiency shown in (C). Reproduced with permission from Ref.[11]. Copyright 2024 American Chemical Society.

$(v=2)$ [57, 58] and NO $(v=2,3)$ [59, 60]. However, due to the microsecond duration of pulsed molecular beams, only a small portion of the beam can be excited by such pulsed lasers. While a cw laser can irradiate the entire molecular beam pulse, its excitation efficiency is generally limited by available power. This limitation can be overcome using a high-finesse optical cavity, which greatly enhances the power of a narrow-linewidth cw laser. This approach has recently been used to saturate molecular overtone transitions [11]. By coupling a milliwatt-level diode laser into a high-finesse cavity, an intra-cavity intensity of 750 kW/cm^2 was achieved, exciting carbon monoxide molecules in a pulsed beam from the ground state to the $v=3$ level via a ro-vibrational transition. An excitation efficiency of up to 35% across the full molecular beam was demonstrated, highlighting the distinct advantage of the cavity-enhanced approach. A detailed description of the method is provided in Ref.[11], while the key results are presented in FIG. 3. Panel (A) shows the ro-vibrational excitation energy levels of CO. The population transfer rate was measured via a depletion method using resonance-enhanced multi-photon ionization (REMPI). Panel (B) provides a schematic of the interaction between the infrared light and the molecular beam. Panel (C) plots the REMPI signal as a function of the scanned infrared laser frequency. Panels (D)–(F) display the corresponding REMPI and depletion signals represented in three-dimensional space, which are essential for performing cross-beam experiments in state-to-state reaction dynamics studies.

Since this method relies fundamentally on infrared transitions, it is applicable to all infrared-active molecules, including CO_2, H_2O, NH_3, CH_4, and even HD, the latter having an extremely high saturation intensity of approximately 0.11 GW/cm^2 for the

DOI: 10.1063/1674-0068/cjcp2511176 © 2026 Chinese Physical Society

$(v = 2, j = 1) \leftarrow (v = 0, j = 0)$ overtone transition [11]. CEE holds great potential to play a crucial role in the fields of molecular quantum state preparation and chemical dynamics.

IV. CEE IN A THREE-LEVEL SYSTEM

A. One-color two-photon spectroscopy

The one-color two-photon spectroscopy method is based on the energy level scheme shown in FIG. 4(a), where the relevant energy levels correspond to molecular vibrational states. Unlike two-photon transitions mediated by electronic states, the weak single-photon transition dipole moment between vibrational states makes non-resonant two-photon transitions extremely weak and difficult to observe. However, the two-photon absorption (TPA) cross section can be significantly enhanced by introducing a near-resonant intermediate state and using high laser power. The use of a high-finesse optical cavity further boosts this process: it not only increases the intra-cavity laser power to meet TPA requirements but also extends the effective interaction path length between the laser and molecules, thereby improving detection sensitivity. Moreover, due to its Doppler-free nature, TPA yields spectral linewidths more than two orders of magnitude narrower than those of single-photon absorption transitions [61, 62].

The concept of one-color two-photon absorption using a single laser was first proposed by Lehmann *et al.* [63, 64] and has recently been experimentally realized by our group [65, 66]. The experimental setup for TPA measurements is similar to that shown in FIG. 1(a). We measure the cavity transmittance at the center frequency ν_0 of the two-photon transition as:

$$\kappa \equiv \frac{P_{\mathrm{ic}}(\nu_0)}{P_{\mathrm{ic},0}}, \tag{8}$$

where P_{ic} and $P_{\mathrm{ic},0}$ denote the intra-cavity laser power with and without two-photon absorption, respectively. The measured line profile is relatively complex, being primarily shaped by the natural linewidth convoluted with transit-time broadening and power broadening. A full numerical analysis is required to accurately describe it [67]. Focusing only on the absorption signal at the transition center, we define the dimensionless TPA signal intensity as:

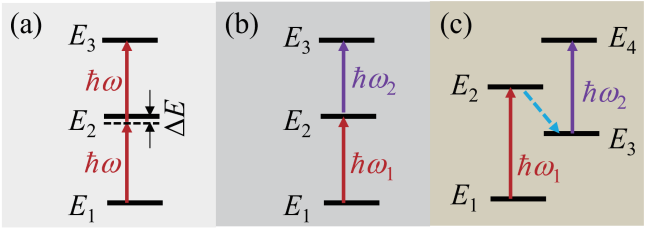

FIG. 4 (a) Energy diagram of a one-color two-photon transition. The intermediate state is detuned by ΔE. The laser photon energy is denoted as $\hbar\omega$. (b) Energy diagram of a two-color double resonance scheme. Photon energies of pump and probe lasers are denoted as $\hbar\omega_1$ and $\hbar\omega_2$, respectively. (c) Double resonance among four-level double resonance (4LDR). The dashed line denotes the non-radiative relaxation process from the E_2 level to E_3.

$$S_{\mathrm{TPA}} \equiv \frac{1-\kappa}{\kappa^2} = \frac{\gamma_2 P_{\mathrm{ic},0}}{\gamma_0}, \tag{9}$$

where γ_2 is the two-photon absorption rate, proportional to the analyte mole fraction [63], $\gamma_0 = c(1-R)/L$ is the empty-cavity loss rate, R is the mirror reflectivity, and L is the cavity length. Based on prior analyses [63, 65], γ_2 depends on the transition parameters, energy level relaxation rates, and molecular concentration. For a given molecular two-photon energy system, all relevant information about γ_2 can be derived after accounting for sample pressure dependence and laser power saturation effects [65]. The TPA signal can be enhanced by using higher-reflectivity and lower-loss mirrors to reduce γ_0, or by increasing the input laser power, before saturation occurs, to raise $P_{\mathrm{ic},0}$.

These experiments validated the quantitative detection capability of this method: measurements of $^{13}CO_2$ samples at various concentrations, cross-verified against isotope ratio mass spectrometry (IRMS), achieved a detection accuracy of 0.5%, meeting the demands of high-precision carbon isotope analysis, as illustrated in FIG. 5. Thanks to its high resolution and narrow linewidth, this approach is particularly suitable for detecting trace molecular isotopes, especially in cases where single-photon absorption is obscured by interfering transitions.

Beyond trace detection, the cavity-enhanced TPA technique also enables precise measurements of molecular vibrational energies. Given that the natural linewidths of many rovibrational transitions can reach the Hertz level or below, this method opens a path toward developing frequency references with exceptional precision. Such advances could support a range of future applications, from tests of fundamental physics to

DOI: 10.1063/1674-0068/cjcp2511176 © 2026 Chinese Physical Society

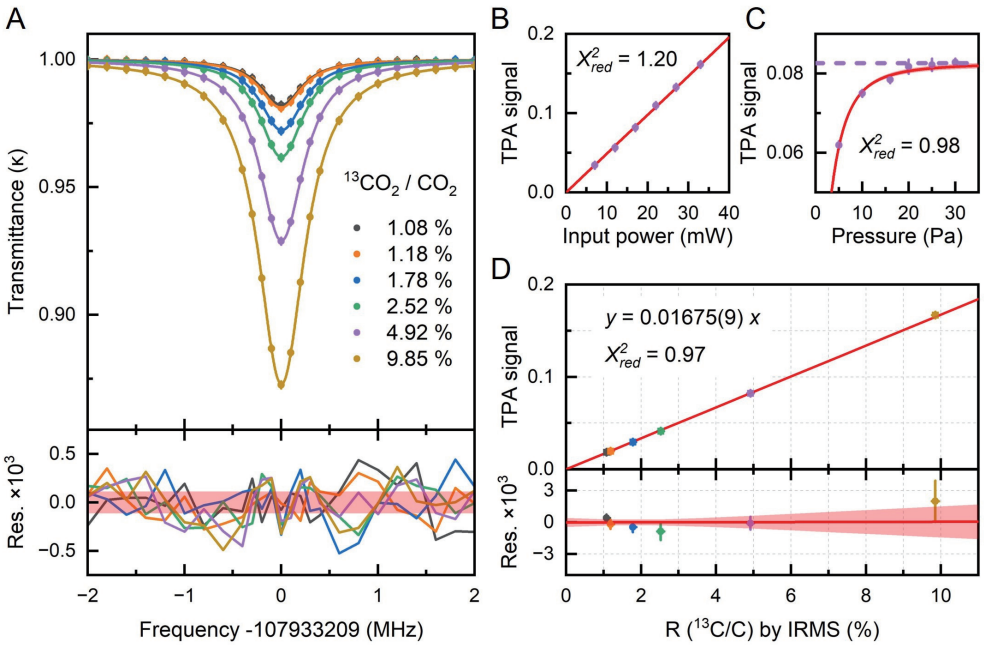

FIG. 5 (A) Experimental TPA spectra (data points) for samples with different $^{13}CO_2$ concentrations, fitted using Voigt profiles (solid lines). Residuals of the fit are displayed in the lower panel. All measurements were performed at a sample pressure of 20 Pa and an input laser power of 17 mW. (B) TPA signal intensity as a function of input laser power at a fixed sample pressure of 20 Pa. The solid line represents a linear fit to the experimental data. (C) TPA signal intensity versus sample pressure at a fixed input power of 17 mW. The solid curve corresponds to a fit based on the TPA model detailed in the Supporting Information of Ref.[65], while the dashed line indicates the high-pressure asymptotic limit. (D) Correlation between the normalized TPA signal (measured at 20 Pa and 17 mW) and the $^{13}C/C$ ratio determined by isotope ratio mass spectrometry (IRMS). Circles represent experimental data, and the red line shows a linear fit. Residuals of the fit are provided in the lower panel. Reproduced with permission from Ref.[65]. Copyright 2025 American Chemical Society.

the establishment of new frequency standards based on molecular infrared transitions.

B. Two-color double-resonance spectroscopy

The double-resonance (DR) method has been widely used in the study of molecular excited states, dynamics, and precision spectroscopy [10, 68, 69]. As illustrated in FIG. 4(b), the stepped double-resonance spectroscopy technique relies on pump-probe interactions among three molecular energy levels. A pump laser excites molecules from the initial state E_1 to an intermediate state E_2, and a probe laser subsequently drives the transition from E_2 to a higher-lying state E_3, thereby probing the population in E_2. Provided that the lifetime of the E_2 state is sufficiently long and relaxation is slow, a condition typically satisfied by ro-vibrational states in most molecules, the probe laser can effectively detect molecules populated on E_2. The double-resonance process suppresses Doppler broadening, yielding extremely narrow transition linewidths. By selecting appropriate double-resonance transitions, interference from other molecular transitions can be minimized, enabling selective detection of specific transitions.

Consider a molecule of rest mass M absorbing a photon of frequency ω in the laboratory frame. Upon excitation, the molecule's velocity changes from $\vec{v}_i$ to $\vec{v}_f$, with an energy difference $\hbar\omega_0$ between the initial and final states. By applying relativistic energy and momentum conservation [70], the resulting velocity change due to photon absorption or emission can be derived. Double-resonance schemes among three energy levels fall into three categories: (i) Λ-type, (ii) V-type, and (iii) Ξ-type (ladder). In Λ-type configurations, two transitions share a common upper state. In V-type schemes, two transitions originate from the same lower state. In Ξ-type (ladder) configurations, the first laser pumps molecules to an intermediate state, and the second laser excites them to a higher state.

Taking the laser propagating direction as the z axis, we can derive the double-resonance conditions for a molecule interacting with two counter-propagating light beams:

DOI: 10.1063/1674-0068/cjcp2511176 © 2026 Chinese Physical Society

For Λ type

$$\frac{\omega_{10}}{\omega_1}-1+\frac{\omega_{20}}{\omega_2}-1=\frac{v^2}{c^2}+\frac{\hbar\omega_1+\hbar\omega_2}{2Mc^2} \tag{10}$$

For V type

$$\frac{\omega_{10}}{\omega_1}-1+\frac{\omega_{20}}{\omega_2}-1=\frac{v^2}{c^2}-\frac{\hbar\omega_1+\hbar\omega_2}{2Mc^2} \tag{11}$$

For Ξ type

$$\frac{\omega_{10}}{\omega_1}-1+\frac{\omega_{20}}{\omega_2}-1=\frac{v^2}{c^2}+\frac{\hbar\omega_1-\hbar\omega_2}{2Mc^2} \tag{12}$$

The first-order Doppler shifts of these two transitions in counter-propagating laser beams have different signs. Consequently, one laser is blue-shifted, and the other one is red-shifted.

Terms in the right side of Eqs. (10)−(12) correspond to the second-order Doppler shift and the recoil shift, respectively. Taking the CO transition at 1.56 μm as an example, the fractional correction due to the recoil effect is 1.5×10^{-11}. The relative second-order Doppler shift is 1×10^{-12} if we use the most probable speed of carbon monoxide at room temperature. Note that contributions from the recoil shift are different for these three types of double resonances. In the ladder-type DR, the recoil shift almost cancels if the two transition frequencies are close. As a comparison, in conventional saturation spectroscopy (Lamb-dip measurement), the recoil effect leads to a doublet [71] instead of a shift. We can change the cavity length to shift the frequencies of cavity modes and both lasers. Double resonance happens when both lasers are resonant with molecules with a specific speed of v_z along counter-propagating lasers.

In principle, DR condition with co-propagating pump and probe light beams could also be considered. In this case, the first-order Doppler shifts in both laser beams have the same sign. We have conditions for all three types of DR with co-propagating beams:

For Λ type

$$\frac{\omega_{10}}{\omega_1}-\frac{\omega_{20}}{\omega_2}=\frac{\hbar\omega_1-\hbar\omega_2}{2Mc^2} \tag{13}$$

For V type

$$\frac{\omega_{10}}{\omega_1}-\frac{\omega_{20}}{\omega_2}=\frac{\hbar\omega_2-\hbar\omega_1}{2Mc^2} \tag{14}$$

For Ξ type

$$\frac{\omega_{10}}{\omega_1}-\frac{\omega_{20}}{\omega_2}=\frac{\hbar\omega_1+\hbar\omega_2}{2Mc^2} \tag{15}$$

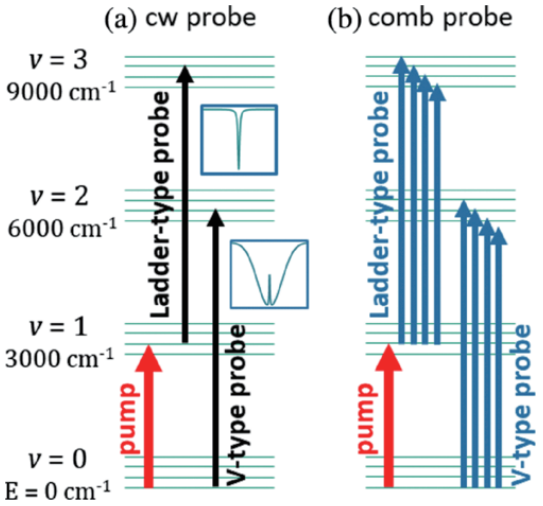

FIG. 6 The energy level structure of the ν_3 C–H stretching bands of methane with pump (red) and probe transitions indicated for (a) a single frequency probe (black) and (b) a frequency comb probe (blue). Reproduced with permission from Ref.[72]. Copyright 2021 American Physical Society.

Therefore, the two lasers must be both blue-shifted or both red-shifted. Note that all the cavity modes move in the same direction when the cavity length changes. We could find that it would be hard to fulfill the DR conditions with co-propagating beams without leaving the two lasers far off-resonance. While in the case of counter-propagating beams, when one laser is slightly blue-shifted and the other laser is red-shifted, we can easily fulfill the DR conditions, Eqs. (10)−(12), with a small change of the cavity length.

Recently, optical-optical double-resonance (DR) spectroscopy using narrow-linewidth lasers has been demonstrated by several research groups. Karhu *et al.* [73–75] used a 3 μm cw laser to pump fundamental band transitions of acetylene and detected symmetric vibrational states via near-infrared cavity ring-down spectroscopy. Foltynowicz *et al.* [72, 76, 77] employed a 3.3 μm cw pump laser and a 1.67 μm optical frequency comb to observe sub-Doppler methane transitions, as shown in FIG. 6. This method reduces spectral linewidths and aids in identifying overtone transitions to highly excited states; however, the measurement accuracy was limited to a few MHz due to pump laser frequency fluctuations and limited detection sensitivity [72]. We have also implemented MIR-NIR double-resonance spectroscopy, determining fundamental and hot band transitions in $^{13}CO_2$ with kilohertz-level accuracy [78].

Since fundamental vibrational transitions in

DOI: 10.1063/1674-0068/cjcp2511176 © 2026 Chinese Physical Society

molecules are relatively strong, a single-pass mid-infrared laser with power on the order of hundreds of milliwatts is generally sufficient to excite the molecules. Hence, resonant enhancement is typically not required for MIR laser excitation. In contrast, near-infrared excitation or detection often employs high-finesse optical cavities to enhance the light-molecule interaction. Hu *et al.* [10, 79] demonstrated comb-locked cavity-assisted double-resonance (coca-DR) spectroscopy, in which both the near-infrared pump and probe lasers are stabilized to the same optical cavity. FIG. 7 shows coca-DR spectra of CO obtained when one laser was resonant with the R(9) line in the (3-0) band while the other was tuned to resonance with the P(10) line in the (6-3) band. This scheme pumps molecules to the excited level ($v = 3$, J=10). The approach enabled, for the first time, the investigation of highly excited vibrational states with kilohertz-level accuracy. The high selectivity of cavity-assisted double-resonance spectroscopy has also been applied to the quantitative detection of trace molecular isotopes, such as $^{14}CO_2$ ($^{14}C/C \simeq 10^{-12}$) in environmental samples [80–82].

After excitation to higher energy levels, molecules can undergo collision-induced relaxation into new excited states, which may then be probed by a second laser. This process gives rise to a four-level double resonance (4LDR) scheme [83], as depicted in FIG. 4(c). Such relaxation has been observed in CH_4 and CO_2, where transfer between excited states is driven by molecular collisions inside the gas cell. These random collisions effectively randomize the initial molecular velocities, largely erasing the velocity selectivity inherent in the standard double-resonance lineshape. As a result, the detected 4LDR spectra become significantly broadened. For instance, Lehmann *et al.* [83] reported that at 0.2 Torr, the 4LDR linewidth becomes comparable to the Doppler-broadened width. Jiang and McCartt [82] also observed the excitation of $^{14}CO_2$ molecules to various rotational levels within the $v_3 = 1$ vibrational state, while the pump laser was resonant with the $v_3 = 1$, $J = 13$ level under conditions of about 2.7 kPa and 300 K. This type of collisional relaxation is particularly useful for studying inelastic collision-induced energy transfer processes between molecules. Despite its simple underlying principle, the DR method has gained considerable prominence in molecular spectroscopy. Its critical applications in complex analysis and high-selectivity detection suggest that it will exert a profound and enduring influence on the field.

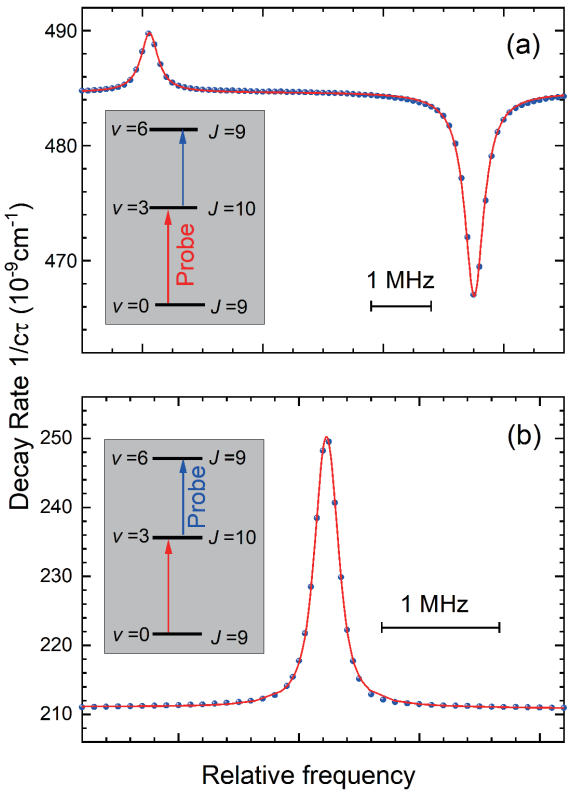

FIG. 7 Comb-locked cavity-enhanced double-resonance (coca-DR) spectrum of the CO molecule. Laser-1 is resonant with the R(9) line in the (3-0) band, and laser-2 is resonant with the P(10) line in the (6-3) band. (a) The spectrum when scanning the frequency of Laser-1. Note the dip represents the saturation spectrum of the R(9) line in the (3-0) band. The distance between the peak (DR signal) and the dip indicate the first-order Doppler shift $\sim \frac{v}{c}\omega_1$. (b) The spectrum when scanning the frequency of Laser-2. Reproduced with permission from Ref.[79]. Copyright 2021 AIP Publishing.

V. PERSPECTIVE

In summary, cavity-enhanced excitation (CEE) techniques are poised to further advance molecular science and precision measurement by leveraging their fundamental advantage: extending light-matter interactions through high-finesse optical cavities. Technologically, continued refinement of high-reflectivity mirror coatings, aimed at minimizing residual absorption and scattering losses, along with the development of cavity geometries, such as microscale whispering-gallery-mode resonators, will push effective optical path lengths beyond the current kilometer scale. This approach facilitates detection sensitivities reaching the sub-ppqv (parts per quadrillion by volume) range, bridging critical technological gaps in applications including trace atmospheric pollutant monitoring.

DOI: 10.1063/1674-0068/cjcp2511176
© 2026 Chinese Physical Society

In terms of application, CEE methods will increasingly integrate with advanced laser systems, including frequency-comb lasers, and quantum sensing platforms such as single-photon detectors. This integration will enhance spectral resolution enough to resolve fine rotation-vibration transitions and enable deterministic measurement of molecular quantum states. Such advances will not only refine quantum chemical models by delivering more accurate data on transition frequencies and oscillator strengths, but also open new frontiers in chemical kinetics and reaction dynamics, such as real-time probing of short-lived reaction intermediates under extreme high-temperature or high-pressure conditions, which have remained inaccessible to conventional spectroscopic methods. The temporal resolution of CEE based on continuous-wave lasers is inherently limited by the cavity buildup time that exceeds 100 μs for high-finesse cavities. To resolve dynamics on shorter timescales, specialized time-gated or pump-probe methodologies must be employed.

Similar to the representative techniques highlighted in this review, the laser power enhancement method has been widely integrated into diverse spectroscopic platforms, driving them toward state-of-the-art performance. Notable examples include recent advances in cavity-enhanced direct frequency comb spectroscopy [84], photoacoustic spectroscopy [85, 86], photothermal spectroscopy [87], and Raman spectroscopy [88–90]. In these applications, CEE is employed to amplify the signal level, thereby substantially improving the overall detection sensitivity. The ongoing miniaturization of CEE-based instruments, for instance, through fiber-coupled compact cavities, will enable field-deployable sensing platforms. Concurrently, synergy with machine learning algorithms will optimize cavity alignment and spectral data interpretation, enhancing both the automation and long-term stability of CEE systems. Ultimately, CEE techniques will solidify their role as versatile cross-disciplinary tools, bridging critical gaps in sensitivity, resolution, and applicability across molecular spectroscopy, environmental science, biomedical diagnostics, and fundamental quantum metrology.

VI. ACKNOWLEDGMENTS

The authors thank Tian-Gang Yang, Xue-Ming Yang, Jin Wang, and Yu Robert Sun for the discussion. This work was jointly supported by the Chinese Academy of Sciences (Grant Nos. YSBR-055, XDB0970100), and the National Natural Science Foundation of China (Nos. 22241302, 12393825).

[1] M. A. R. Reber, Y. Chen, and T. K. Allison, Optica **3**, 311 (2016).
[2] A. H. Zewail, Angew. Chem. Int. Ed. **39**, 2586 (2000).
[3] S. Y. T. van de Meerakker, H. L. Bethlem, N. Vanhaecke, and G. Meijer, Chem. Rev. **112**, 4828 (2012).
[4] L. D. Carr, D. DeMille, R. V. Krems, and J. Ye, New J. Phys. **11**, 055049 (2009).
[5] N. V. Vitanov, A. A. Rangelov, B. W. Shore, and K. Bergmann, Rev. Mod. Phys. **89**, 015006 (2017).
[6] M. C. Silfies, G. Kowzan, N. Lewis, and T. K. Allison, Phys. Chem. Chem. Phys. **23**, 9743 (2021).
[7] C. Hallas, L. Anderegg, N. B. Vilas, Y. Liu, and J. M. Doyle, Phys. Rev. Lett. **130**, 263001 (2023).
[8] L. S. Ma, J. Ye, P. Dube, and J. L. Hall, J. Opt. Soc. Am. B **16**, 2255 (1999).
[9] L. Gianfrani, S. M. Hu, and W. Ubachs, Riv. Nuovo Cimento **47**, 229 (2024).
[10] C. L. Hu, V. I. Perevalov, C. F. Cheng, T. P. Hua, A. W. Liu, Y. R. Sun, Y. Tan, J. Wang, and S. M. Hu, J. Phys. Chem. Lett. **11**, 7843 (2020).
[11] Q. H. Liu, H. Zhang, L. Wen, Y. Xie, T. Yang, C. F. Cheng, S. M. Hu, and X. Yang, J. Phys. Chem. Lett. **15**, 9926 (2024).
[12] H. Guo and K. Liu, Chem. Sci. **7**, 3992 (2016).
[13] H. Elferink, M. E. Severijnen, J. Martens, R. A. Mensink, G. Berden, J. Oomens, F. P. J. T. Rutjes, A. M. Rijs, and T. J. Boltje, J. Am. Chem. Soc. **140**, 6034 (2018).
[14] H. Pan, B. Zhao, H. Guo, and K. Liu, J. Phys. Chem. Lett. **14**, 10412 (2023).
[15] Y. Bao, X. Liu, T. Rosenband, and K. K. Ni, PRX Quantum **5**, 020344 (2024).
[16] J. Wang, Y. R. Sun, L. G. Tao, A. W. Liu, T. P. Hua, F. Meng, and S. M. Hu, Rev. Sci. Instrum. **88**, 043108 (2017).
[17] A. Okeefe and D. A. G. Deacon, Rev. Sci. Instrum. **59**, 2544 (1988).
[18] P. Zalicki and R. N. Zare, J. Chem. Phys. **102**, 2708 (1995).
[19] D. Romanini, A. A. Kachanov, N. Sadeghi, and F. Stoeckel, Chem. Phys. Lett. **264**, 316 (1997).
[20] S. S. Brown, Chem. Rev. **103**, 5219 (2003).
[21] J. Morville, D. Romanini, A. A. Kachanov, and M. Chenevier, Appl. Phys. B **78**, 465 (2004).
[22] B. A. Paldus and A. A. Kachanov, Can. J. Phys. **83**, 975 (2005).
[23] H. F. Huang and K. K. Lehmann, Opt. Express **15**, 8745 (2007).
[24] B. Gao, W. Jiang, A. W. Liu, Y. Lu, C. F. Cheng, G. S. Cheng, and S. M. Hu, Rev. Sci. Instrum. **81**, 043105 (2010).
[25] H. Pan, C. F. Cheng, Y. R. Sun, B. Gao, A. W. Liu,

DOI: 10.1063/1674-0068/cjcp2511176 © 2026 Chinese Physical Society

and S. M. Hu, Rev. Sci. Instrum. **82**, 103110 (2011).
[26] K. J. Schulz and W. R. Simpson, Chem. Phys. Lett. **297**, 523 (1998).
[27] N. van Leeuwen, J. C. Diettrich, and A. C. Wilson, Appl. Opt. **42**, 3670 (2003).
[28] B. J. Orr and Y. He, Chem. Phys. Lett. **512**, 1 (2011).
[29] R. W. P. Drever, J. L. Hall, F. V. Kowalski, J. Hough, G. M. Ford, A. J. Munley, and H. Ward, Appl. Phys. B **31**, 97 (1983).
[30] Z. T. Zhang, Y. Tan, J. Wang, C. F. Cheng, Y. R. Sun, A. W. Liu, and S. M. Hu, Opt. Lett. **45**, 1013 (2020).
[31] Z. T. Zhang, C. F. Cheng, S. M. Hu, Y. Sun, and A. W. Liu, Opt. Express **28**, 27600 (2020).
[32] Y. D. Tan, J. J. Chen, Y. Zhou, C. F. Cheng, and S. M. Hu, Chin. J. Chem. Phys. **37**, 147 (2024).
[33] J. Wang, Y. R. Sun, L. G. Tao, A. W. Liu, and S. M. Hu, J. Chem. Phys. **147**, 091103 (2017).
[34] G. Giusfredi, S. Bartalini, S. Borri, P. Cancio, I. Galli, D. Mazzotti, and P. De Natale, Phys. Rev. Lett. **104**, 110801 (2010).
[35] D. Gatti, R. Gotti, A. Gambetta, M. Belmonte, G. Galzerano, P. Laporta, and M. Marangoni, Sci. Rep. **6**, 27183 (2016).
[36] T. P. Hua, Y. R. Sun, J. Wang, C. L. Hu, L. G. Tao, A. W. Liu, and S. M. Hu, Chin. J. Chem. Phys. **32**, 107 (2019).
[37] S. Twagirayezu, G. E. Hall, and T. J. Sears, J. Chem. Phys. **149**, 154308 (2018).
[38] Y. Tan, T. P. Hua, J. D. Tang, J. Wang, A. W. Liu, Y. R. Sun, C. F. Cheng, and S. M. Hu, J. Phys. Conf. Ser. **2439**, 012007 (2023).
[39] L. G. Tao, A. W. Liu, K. Pachucki, J. Komasa, Y. R. Sun, J. Wang, and S. M. Hu, Phys. Rev. Lett. **120**, 153001 (2018).
[40] F. M. J. Cozijn, P. Dupré, E. J. Salumbides, K. S. E. Eikema, and W. Ubachs, Phys. Rev. Lett. **120**, 153002 (2018).
[41] J. Ye, L. S. Ma, and J. L. Hall, J. Opt. Soc. Am. B **15**, 6 (1998).
[42] T. P. Hua, R. Y. Sun, and S. M. Hu, Opt. Lett. **45**, 4863 (2020).
[43] M. L. Diouf, F. M. J. Cozijn, B. Darquié, E. J. Salumbides, and W. Ubachs, Opt. Lett. **44**, 4733 (2019).
[44] Y. N. Lv, A. W. Liu, Y. Tan, C. L. Hu, T. P. Hua, X. B. Zou, Y. R. Sun, C. L. Zou, G. C. Guo, and S. M. Hu, Phys. Rev. Lett. **129**, 163201 (2022).
[45] F. M. J. Cozijn, M. L. Diouf, W. Ubachs, V. Hermann, and M. Schlösser, Phys. Rev. Lett. **132**, 113002 (2024).
[46] F. M. J. Cozijn, M. L. Diouf, and W. Ubachs, Phys. Rev. Lett. **131**, 073001 (2023).
[47] Q. H. Liu, Y. Tan, C. F. Cheng, and S. M. Hu, Phys. Chem. Chem. Phys. **25**, 27914 (2023).
[48] N. D, R. Judson, D. Kouri, D. Adelman, N. Shafer, D. Kliner, and R. Zare, Science **257**, 519 (1992).
[49] T. Kitsopoulos, M. Buntine, D. Baldwin, R. Zare, and D. Chandler, Science **260**, 1605 (1993).
[50] Y. Segev, N. Bibelnik, N. Akerman, Y. Shagam, A. Luski, M. Karpov, J. Narevicius, and E. Narevicius, Sci. Adv. **3**, e1602258 (2017).
[51] L. Schnieder, K. Seekamprahn, J. Borkowski, E. Wrede, K. Welge, F. Aoiz, L. Banares, M. Dmello, V. Herrero, V. Rabanos, and R. Wyatt, Science **269**, 207 (1995).
[52] S. Harich, D. Dai, C. Wang, X. Yang, S. Chao, and R. Skodje, Nature **419**, 281 (2002).
[53] G. Tang, M. Besemer, S. Kuijpers, G. C. Groenenboom, A. van der Avoird, T. Karman, and S. Y. T. van de Meerakker, Science **379**, 1031 (2023).
[54] T. Wang, J. Chen, T. Yang, C. Xiao, Z. Sun, L. Huang, D. Dai, X. Yang, and D. H. Zhang, Science **342**, 1499 (2013).
[55] T. Yang, J. Chen, L. Huang, T. Wang, C. Xiao, Z. Sun, D. Dai, X. Yang, and D. H. Zhang, Science **347**, 60 (2015).
[56] H. Pan and K. Liu, Nat. Chem. **14**, 545 (2022).
[57] P. R. Shirhatti, I. Rahinov, K. Golibrzuch, J. Werdecker, J. Geweke, J. Altschaeffel, S. Kumar, D. J. Auerbach, C. Bartels, and A. M. Wodtke, Nat. Chem. **10**, 592 (2018).
[58] A. Kumar, S. K. Singh, and P. R. Shirhatti, Rev. Sci. Instrum. **94**, 113001 (2023).
[59] K. Golibrzuch, P. R. Shirhatti, J. Altschaeffel, I. Rahinov, D. J. Auerbach, A. M. Wodtke, and C. Bartels, J. Phys. Chem. A **117**, 8750 (2013).
[60] K. Golibrzuch, P. R. Shirhatti, I. Rahinov, D. J. Auerbach, A. M. Wodtke, and C. Bartels, Phys. Chem. Chem. Phys. **16**, 7602 (2014).
[61] L. S. Vasilenko, V. P. Chebotaev, and A. V. Shishaev, JETP Lett. **12**, 113 (1970).
[62] F. Biraben, B. Cagnac, and G. Grynberg, Phys. Rev. Lett. **32**, 643 (1974).
[63] K. K. Lehmann, J. Chem. Phys. **151**, 144201 (2019).
[64] K. K. Lehmann, Appl. Phys. B **116**, 147 (2014).
[65] Y. Z. Liu, M. Y. Yu, Y. D. Tan, J. Wang, C. F. Cheng, W. Jiang, and S. M. Hu, Anal. Chem. **97**, 848 (2025).
[66] Y. Z. Liu, W. T. Cai, Y. D. Tan, T. P. Hua, C. F. Cheng, and S. M. Hu, Appl. Phys. B **131**, 99 (2025).
[67] K. K. Lehmann, J. Chem. Phys. **154**, 104105 (2021).
[68] A. Callegari, H. Srivastava, U. Merker, K. Lehmann, G. Scoles, and M. Davis, J. Chem. Phys. **106**, 432 (1997).
[69] C. H. Zhang and G. H. Sha, Science **262**, 374 (1993).
[70] W. Demtröder, *Laser Spectroscopy: Basic Concepts and Instrumentation*, 4th Edn., Berlin: Springer, (2008).
[71] J. L. Hall, C. J. Bordé, and K. Uehara, Phys. Rev. Lett. **37**, 1339 (1976).
[72] A. Foltynowicz, L. Rutkowski, I. Silander, A. C. Johansson, V. S. de Oliveira, O. Axner, G. Soboń, T. Martynkien, P. Mergo, and K. K. Lehmann, Phys. Rev. Lett. **126**, 063001 (2021).
[73] J. Karhu, J. Nauta, M. Vainio, M. Metsälä, S. Hoek-

DOI: 10.1063/1674-0068/cjcp2511176 © 2026 Chinese Physical Society

stra, and L. Halonen, J. Chem. Phys. **144**, 244201 (2016).
[74] J. Karhu, M. Vainio, M. Metsälä, and L. Halonen, Opt. Express **25**, 4688 (2017).
[75] J. Karhu, K. Lehmann, M. Vainio, M. Metsälä, and L. Halonen, Opt. Express **26**, 29086 (2018).
[76] A. Foltynowicz, L. Rutkowski, I. Silander, A. C. Johansson, V. S. de Oliveira, O. Axner, G. Soboń, T. Martynkien, P. Mergo, and K. K. Lehmann, Phys. Rev. A **103**, 022810 (2021).
[77] V. S. de Oliveira, I. Silander, L. Rutkowski, G. Soboń, O. Axner, K. K. Lehmann, and A. Foltynowicz, Nat. Commun. **15**, 161 (2024).
[78] Y. D. Tan, C. F. Cheng, Y. Tan, and S. M. Hu, Opt. Lett. **49**, 1109 (2024).
[79] C. L. Hu, J. Wang, T. P. Hua, A. W. Liu, Y. R. Sun, and S. M. Hu, Rev. Sci. Instrum. **92**, 073003 (2021).
[80] Y. D. Tan, C. F. Cheng, D. Sheng, and S. M. Hu, Chin. J. Chem. Phys. **34**, 373 (2021).
[81] J. Jiang and A. D. McCartt, J. Chem. Phys. **155**, 104201 (2021).
[82] J. Jiang and A. D. McCartt, Proc. Natl. Acad. Sci. USA **121**, e2314441121 (2024).
[83] K. K. Lehmann, A. Hjältén, I. Silander, M. Rey, and A. Foltynowicz, J. Chem. Phys. **163**, 144304 (2025).
[84] P. Mas lowski, K. Cossel, A. Foltynowicz, and J. Ye, *Cavity-Enhanced Direct Frequency Comb Spectroscopy*, Berlin, Heidelberg: Springer, 271–321 (2014).
[85] Q. Nie, Z. Wang, K. Duan, M. Hu, M. Du, and W. Ren, Opt. Lett. **49**, 3648 (2024).
[86] K. Zheng, W. Luo, L. Duan, S. Zhao, S. Jiang, H. Bao, H. L. Ho, C. Zheng, Y. Zhang, W. Ye, and W. Jin, Sens. Actuat. B **415**, 135984 (2024).
[87] Y. Yan, X. Xiao, Q. Nie, Z. Wang, Y. Chen, J. Wu, N. Zhou, R. Zhou, S. Yang, and W. Ren, Laser Photon. Rev. **18**, 2400907 (2024).
[88] Q. Y. Yang, Y. Tan, Z. H. Qu, Y. R. Sun, A. W. Liu, and S. M. Hu, Anal. Chem. **95**, 5652 (2023).
[89] P. Wang, W. Chen, J. Wang, Y. Lu, Z. Tang, and Y. Tan, Anal. Chem. **95**, 6894 (2023).
[90] Q. Nie, G. Lyu, C. Wei, and W. Ren, Laser Photon. Rev. **20**, e01645 (2025).

DOI: 10.1063/1674-0068/cjcp2511176 © 2026 Chinese Physical Society